Available online at www.sciencedirect.com
SCIENCE DIRECT®
Journal of Non-Crystalline Solids 351 (2005) 1003–1013
JOURNAL OF NON-CRYSTALLINE SOLIDS
www.elsevier.com/locate/jnoncrysol

Medium-range structure in glasses and low-Q structure in neutron and X-ray scattering data

Philip H. Gaskell

Cavendish Laboratory, University of Cambridge, Madingley Road, Cambridge CB3 0HE, UK

Abstract

Attempts to understand the medium-range structure of glasses and other amorphous materials from X-ray and neutron scattering data necessarily focus on the low-Q region, where Q is the modulus of the scattering vector. Data for Q in the range 8–20 nm^{-1} reveal real-space detail on a scale $2\pi/Q$. This corresponds to the region often denoted as 'medium-range structure', 0.5–1.5 nm. An attempt is made to describe the origin of low-Q structure in terms of spatial correlation of atomic density fluctuations and to delineate the inter-atomic distances involved. Amorphous silicon and silica are considered in detail showing that real-space data extending to about 1.1 and 1.6 nm, respectively, are required to specify accurately the detail in the first peaks of the structure factor. The degree of order associated with spatial atomic density fluctuations then becomes a key question. Completely random fluctuations seem unlikely to offer an explanation. Aperiodic, non-crystallographic packing offers some promise, but remains inadequately tested. The most satisfactory results for simple oxide glasses, at least, come from medium-range organization based on the principles underlying compositionally and thermodynamically equivalent crystalline structures. Low-Q structures in neutron scattering data for lithium, sodium and lithium/potassium disilicate glasses are treated as examples.

1. Introduction

Atomic models for the glassy state are intimately linked to structural reasons underlying avoidance of crystal nucleation during cooling from the melt. Is a glass a liquid structure minus some of the dynamics? Are crystallographic ordering processes dominant, even though crystallization, ultimately, must be avoided? Do glasses, and liquids, exist because their structures are based on *non*-crystallographic ordering? Answers exist for the local structure: organization of nearest and next-nearest neighbors is closely related to the principles exhibited by equivalent crystals. A similar statement applied to the medium-range structure is regarded as controversial, however.

One of the most promising clues comes from structure in low angle neutron and X-ray scattering data in amorphous solids, polymers and some liquids. This is often called the First Sharp Diffraction peak (FSDP) or, more generally, low-Q structure (LQS) for Q values in the range 5–20 nm^{-1}. (Here, $Q = |\mathbf{Q}| = 4\pi \sin\theta/\lambda$ is the modulus of the scattering vector, with 2θ, the scattering angle and λ the wavelength of the probing radiation.) The origins of these features have been hotly debated for at least 20 years, although it *is* agreed that they characterize the medium range structure. This paper reviews the impact of several possible explanations involving *spatial correlation* of voids, large ring structures, and 'quasi-lattice planes'. These are intimately interrelated, being different facets of the medium-range structure. An attempt is made to answer the underlying question concerning the form of the spatial correlation in terms of these models.

E-mail address: phg1@cam.ac.uk

0022-3093/$ - see front matter © 2005 Elsevier B.V. All rights reserved.
doi:10.1016/j.jnoncrysol.2005.01.011

2. What is 'low-Q structure'?

I am not aware of any agreed formal definition of the FSDP. Every diffraction pattern must have a first peak and some first peaks are sharp with high intensity. Some are not. Some are barely noticeable broad shoulders in the wings of the second peak. In some materials, like a-$Ag_2Ge_2S_3$, LQS is present in neutron scattering but with no sign of even a shoulder in X-ray scattering (including differential anomalous scattering). In many cases the low-Q structure consists of two or more components. In chalcogenides the temperature- and/or pressure-dependence of the intensity may be anomalous. Perhaps the most challenging aspect is the difficulty of reproducing the FSDP in model structures for some, but not all materials. Although FSDPs in a-SiO_2 and a-GeO_2 are prominent features in X-ray and neutron scattering data, few models represent them accurately. Real-space data, however, can be more acceptably modeled. Some workers have artificially removed the FSDP from the diffraction data and then transformed to real space only to find that the effects of such removal are difficult to characterize – 'subtle' changes only. For amorphous elemental solids like a-Si and a-Ge, on the other hand, the first peak is clearly related to details in the near-neighbor distribution functions and LQS can be simulated more successfully. It seems sensible therefore, to draw a distinction between these elements and their amorphous oxides.

In amorphous metals and molten alloys, LQS is often described in terms of 'pre-peaks'. This raises the question: what is the nature of the 'peak' which is preceded by the LQS? In some cases it is possible to describe the structure factor directly from the inter-atomic potential. The Percus–Yevick formalism treats pair-wise interactions and some higher order terms. For dense randomly packed hard spheres (DRPHS), the simple potential, together with constraints resulting from dense packing, allows an exact solution. This defines the first 'normal' peak in the structure factor, $S(Q)$. Any feature that precedes it can then be termed a pre-peak.

If this is adopted as a reasonable definition, it can be extended to network glasses. A peak in $S(Q)$ that directly and obviously relates to the real-space structure based on the inter-atomic potential with the constraint of network continuity, could be recognized as the first normal peak. Anything that precedes it, becomes low-Q structure. Few inter-atomic interactions used in modeling amorphous materials extend beyond next nearest neighbors, apart from Coulombic terms, and general repulsive terms designed to avoid overlap. It follows that the proposed, tighter, definition focuses on the local structure – extending to, say, third neighbors. The FSDP in silica and similar materials is a pre-peak on this definition, whereas first peaks in amorphous elemental tetrahedral solids are not, as the following analysis suggests.

Low-Q structure results from atomic density fluctuations on a length scale characterized by $2\pi/Q_1$, where Q_1 is the position of the first component of the LQS (or the FSDP). Real and reciprocal space functions are related through Fourier sine transforms:

$$F(Q) = \int_0^\infty G(r)\sin(Qr)\,\mathrm{d}r \tag{1a}$$

and

$$G(r) = \frac{2}{\pi}\int_0^\infty F(Q)\sin(rQ)\,\mathrm{d}Q. \tag{1b}$$

Here, $G(r) = 4\pi r(\rho(r) - \rho_0)$, with $\rho(r)$, the r-dependent atomic density and ρ_0, the average atom density. $F(Q) = Q(S(Q) - 1)$ with $S(Q) = I(Q)/Nb^2$, $I(Q)$ being the scattered intensity at Q for N atoms with scattering length b. (Note that this definition applies to elemental systems only.)

Eq. (1a) shows that for $G(r)$ in the form of a δ function at R, $F(Q)$ is an infinite sine wave with period $\Delta Q = 2\pi/R$. The first maximum at $Q_1 = (2\pi/R)/4$ is not observed due to overlapping contributions from features at higher R values. The first noticeable peak occurs at $5(2\pi/R)/4$, so that $Q_1 = 2.5\pi/R$. Similarly, Eq. (1b) indicates that a δ function at Q_1 in $F(Q)$ generates a sinusoidal $G(r)$ function with period $\Delta r = 2\pi/Q_1$ and vice versa.

2.1. Amorphous silicon and amorphous ice

For a Gaussian function in $G(r)$ centered at R, with standard deviation σ, the sine function is modified by an exponential window function so that

$$F(Q) \propto \sin(QR)\exp -(Q^2\sigma^2)/2. \tag{2}$$

Etherington et al. [1] have shown fitting parameters describing nearest and next-nearest Ge–Ge distributions in a-Ge inserted into this equation gives a reasonable approximation to the FSDP at about 20 nm^{-1}. Parameters fitting the corresponding real-space peaks in the X-ray data for a-Si (Laaziri et al. [2]) give a similar fit compared to the experimental $F(Q)$ data. Specifically, the second neighbor Si–Si distribution centered on 0.38 nm produces a sinusoidal oscillation with a peak at $2.5\pi/0.38 = 20.6$ nm^{-1} as observed. Inter-atomic potentials for a-Si extend to second neighbors of course. For a-SiO_2, $Q_1 = 15.2 = 2.5\pi/R$ nm^{-1} suggesting contributions from a peak centered at $R = 0.52$ nm. This is well beyond the third neighbor (Si–Si(1)) distance which is the limit for many potential functions, and corresponds to O–O(2) and Si–Si(2) distributions. These could perhaps be modeled by specifying dihedral angle or ring size distributions but would otherwise be functions of (random) network constraints only.

A more revealing approach is to calculate $S^*(Q) = 1 + F^*(Q)/Q$ from Eq. (1a) with a truncated transform: that is

$$F^*(Q) = \int_0^{R\max} G(r)\sin(Qr)\,dr \qquad (3)$$

with R_{max} chosen to lie at an even node of $G(r)$ to avoid spurious ripple. With R_{max} = 0.55 nm, Fig. 1(a), the first and second peaks of $G(r)$ for a-Si are included in the transform, and much of the first peak in $S(Q)$ at 20 nm^{-1} is reproduced, Fig. 1(b). Increasing R_{max} to about 0.9 nm gives an even better fit to experimental data. These findings conflict in detail with the conclusions of Uhlherr and Elliott [3]. They have claimed that almost half of the contribution to the FSDP in a-Si comes from 'extended range ordering', which is observed as very low amplitude oscillations extending beyond 1 nm to about 4 nm in real-space data derived from a large model for a-Si devised by Holender and Morgan [4]. By contrast, the results quoted here show that the largest contribution to the FSDP is defined by details of the local structure: specifically the *tetrahedrality* of Si, which is determined, in turn, by the strong covalent Si–Si bond. However, accurate specification of the height and width of the FSDP requires higher Fourier components present in real space data to about 1.6 nm, as discussed below.

Amorphous ice is thought to have a random network structure like a-Si. Fitting parameters for the first two peaks were obtained by Narten et al. [5] from an analysis of the high-Q region of $S(Q)$ of their X-ray data. While these values may be less accurate than fits to the real-space distribution functions, values of $F(Q)$ calculated using Eq. (2) again give a reasonable representation of the FSDP. Transforming $G(r)$ data including only the first two peaks (R_{max} = 0.61 nm), Fig. 2, produces a reasonable fit, Fig. 3, to $S(Q)$ (which is dominated by O–O correlations). Fig. 3 also shows that differences seen in the 'FSDP' between low- and high-density amorphous ice are also interpretable in terms of differences in the near neighbor $G(r)$ data. It may still be legitimate to describe the changes in the 'FSDP' in terms of the void-void structure as proposed by Elliott [6], and

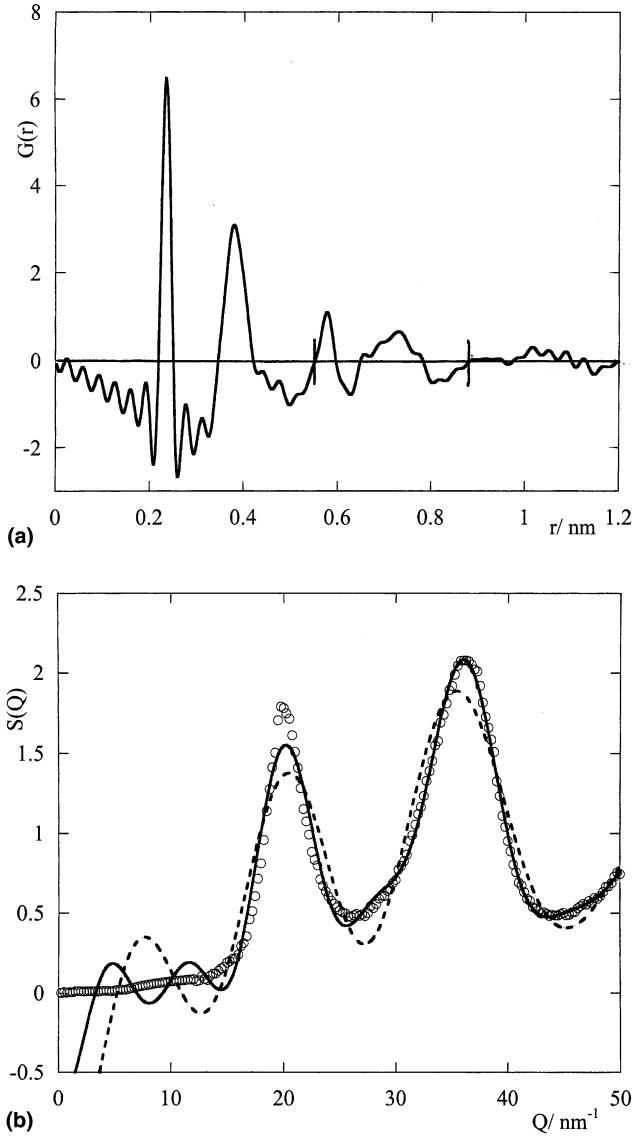

Fig. 1. (a) $G(r)$ for a-Si (annealed) calculated from experimental $S(Q)$ data [2]. Values of R_{max} (see Eq. (3)) are marked. (b) $S^*(Q)$ calculated using a Fourier transform of $G(r)$ truncated at two values of R_{max} (see Eq. (3)). R_{max} = 0.552 nm (dashed line); R_{max} = 0.9 nm (full line), compared to experimental $S(Q)$ data [2] (points). Note that a good approximation to the experimental FSDP at 20 nm^{-1} is obtained from $G(r)$ data extending to second neighbors only, but that it is still not completely reproduced for R_{max} = 0.9 nm.

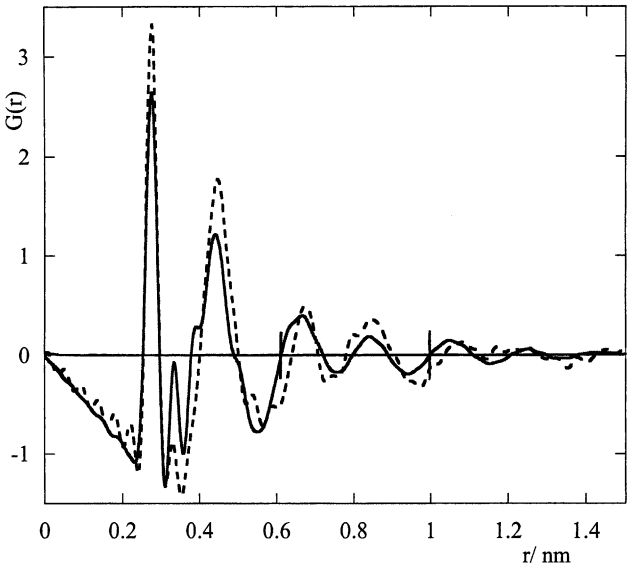

Fig. 2. $G(r)$ data calculated from experimental X-ray $S(Q)$ data for two forms of amorphous ice (Narten et al. [5]). Specimens condensed at 77 K (dashed line) and at 10 K (full line). Values of R_{max} are marked. Note the increased intensity of the feature at about 0.35 nm in the 10 K specimen.

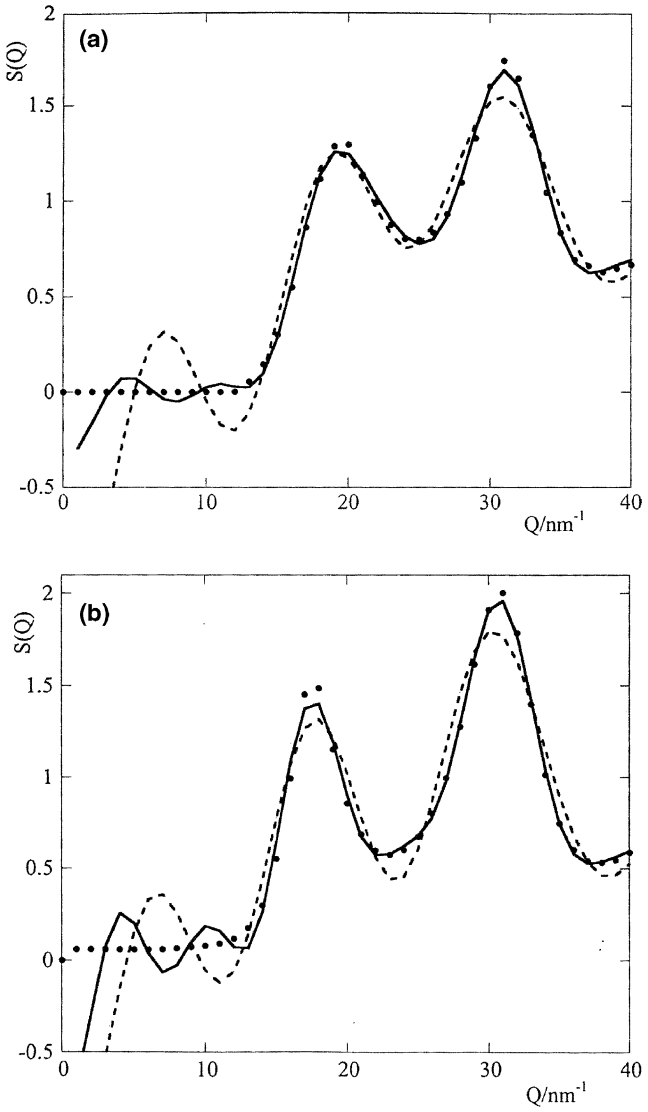

Fig. 3. $S(Q)$ data for a-ice condensed at: (a) 10 K; (b) 77 K. $S^*(Q)$ was calculated from a Fourier transform of $G(r)$ truncated at about 0.6 nm (dashed line) and 1.0 nm (full line), compared to experimental $S(Q)$ data [5] (points). Note that the first peaks near 20 and 18 nm^{-1} are adequately reproduced by $G(r)$ data extending to about 0.6 nm and thus including second neighbors only. (The peak in $G(r)$ in Fig. 2 at about 0.35 nm is thought to be due to interstitial H_2O molecules.)

Barker et al. [7]. However, the advantages offered by this approach are not obvious.

Since tetrahedrality applies to the molecular centers (strictly to O–O intermolecular correlations) it cannot be strictly classified as 'local' structural ordering in line with the tighter definition of low-Q structure proposed here. H–H and O–H correlations are also involved with weak O–O interactions, presumably. More generally, it then becomes debatable whether the first peaks in $S(Q)$ for structures like liquid or amorphous methane or liquid ethanol, or even amorphous polymers like polyethylene should be treated as FSDPs. Clearly, interpretation through real-space distributions is far less straightforward than for a-ice, due to the overlapping contributions from 'local' C–H, H–H and O–H intramolecular correlations. But intermolecular correlations are responsible for the first peak and these are often modeled through analytic solutions – like the Percus–Yevick formulation – to the properties of packed spheres.

2.2. Amorphous SiO_2 and GeO_2

The contrast between the amorphous tetrahedral semiconductors and a-SiO_2 and GeO_2 is marked. The latter also contain tetrahedral elements, T, but insertion of the inter-tetrahedral oxygens result in first neighbor T–T distributions that are drastically broadened. There is a wide spread of oxygen bond angles ($\sigma \sim 15°$) and only limited constraints imposed by network continuity on T–T–T dihedral angles [8]. The first three peaks in the real-space distribution function specify the T–O(1), O–O(1) and T–T(1) correlations. Inserting fitting parameters for these peaks into Eq. (2) gives a reasonable good fit to all the features in the reciprocal space data *except for* $Q < 30$ nm^{-1}. The FSDP is not seen at all.

Inversion of $G(r)$ function truncated at 0.46 nm – thus including the Si–O(2) and O–O(2) correlations (Fig. 4(a)) produces a very broad feature centered close to the position of the FSDP at 15.2 nm^{-1}, in the experimental neutron scattering data [9] Fig. 4(b). Increasing R to 0.6 nm and thus including the feature near to $2\pi/Q_1 = 0.52$ nm, referred to above, gives an approximation to the FSDP but with lower accuracy than that produced for a-Si by inclusion of second neighbors only. A good fit again requires Fourier inversion of real-space data to about 1.1 nm.

Similar results come from continuous random network models for a-GeO_2 constructed by Wefing [10] using carefully controlled constraints on medium-range parameters such as ring-size distributions, minimum distances for non-bonded atoms. This is additional to control of nearest-neighbor bond length and angle distributions. The resulting models give good fits to experimental r-space data (the correlation factor is about 0.3 over the range 0–1 nm). However, the FSDP at 16 nm^{-1} is significantly broader than the experimental data of Desa et al. [11]. The reason presumably lies in inaccurate representation of medium-range constraints. In particular, the dihedral angle was unconstrained in most of the simulations, although a note is made of some simulations in which staggered configurations are preferred. Unfortunately, Q-space data is not quoted.

Amorphous $ZnCl_2$ provides an further example. Desa et al. [12] showed that fitting parameters for the first two peaks (Zn–Cl and Cl–Cl) give a good representation of a strong first peak in $S(Q)$ at about 21 nm^{-1}, but there is no indication of the weak pre-peak observed at about 11 nm^{-1}. This peak also survives in the liquid state, as in other zinc halides.

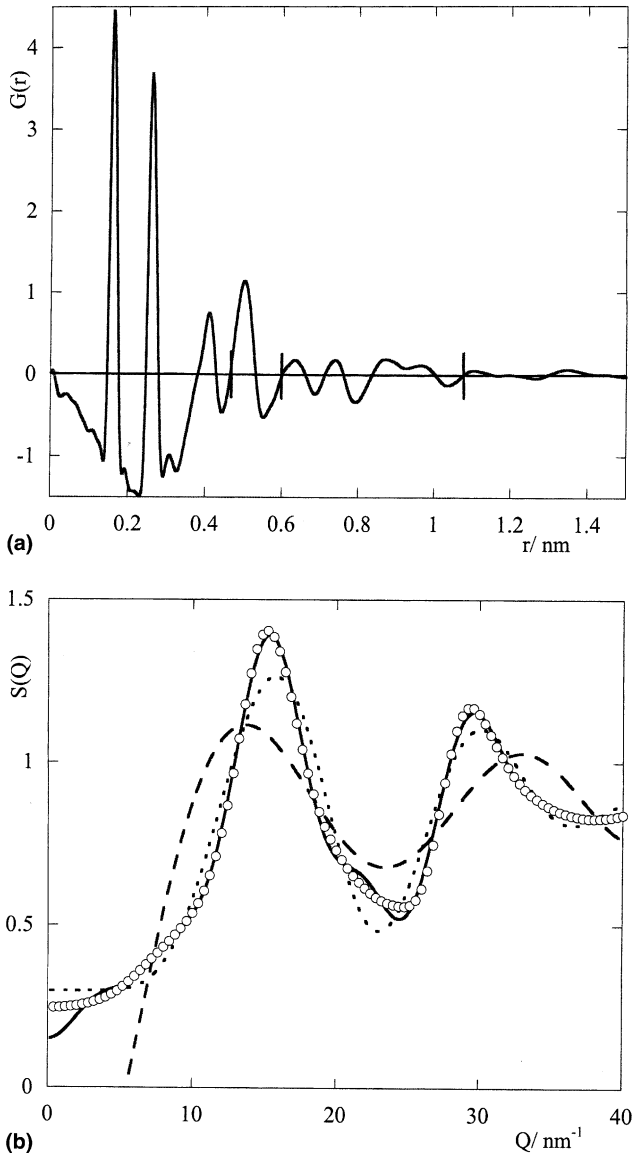

Fig. 4. (a) $G(r)$ for a-SiO_2 calculated from experimental neutron $S(Q)$ data [9]. Values of R_{max} at 0.47, 0.60 nm and 1.08 nm are marked. Note that R_{max} = 0.47 nm includes the first five peaks – the Si–Si(1) peak at about 0.3 nm is not strongly weighted in neutron scattering data. (b) $S^*(Q)$ calculated using Fourier transforms of $G(r)$ truncated at 0.47 nm (dashed line); 0.60 nm (dotted line) and 1.08 nm (full line). Experimental $S(Q)$ data [9] are represented by points.

3. Origins of low-Q structure

In Section 2, it was pointed out that LQS could be the result of a sharp peak in $G(r)$ at $2.5\pi/R$, and of (damped) sinusoidal oscillations in $G(r)$ with a period $\Delta r = 2\pi/Q_1$. Are either of these mechanisms responsible for LQS? In a-Si and a-ice considered above, the first peak in the reciprocal space data is related primarily to a sharp peak in $G(r)$. But although the local structure of a-Si and a-ice produce the dominant contributions to $S(Q_1)$, medium-range contributions are essential to furnish accurate representations of the detail – specifically the height and the width of the $S(Q_1)$ distribution. Fourier transform of $G(r)$ data for a-Si extending to R_{max} = 1.6 nm is required to specify the first peak to a similar degree of accuracy as that for silica with R_{max} = 1.08 nm. In other words, while the first peak for a-Si is quite well-defined by the second neighbor distribution beginning at about 0.3 nm, detail in $G(r)$ is required over a length scale that is about 60% greater than that for silica.

In a-SiO_2 and GeO_2, the signature of LQS in $G(r)$ still requires complete decoding. Gaskell and Wallis [13] showed that in a-SiO_2, *conjunctions* of particular distances represented in the *set* of features apparent in $G(r)$ out to about 1.1 nm are implicated. To explain this, we consider first the general situation for atom scattering in any material, crystalline or amorphous: then, a simpler, but closely related case, c-Si.

Fig. 5, shows an incident plane wave of neutrons scattered from atom α, position vector $\mathbf{r}_\alpha$, with an amplitude:

$$A_\alpha(\mathbf{Q}) \propto b_A \exp i(\mathbf{Q}\cdot\mathbf{r}_\alpha). \tag{4}$$

$\mathbf{Q}\cdot\mathbf{r}_\alpha$, the projection of $\mathbf{r}_\alpha$ on $\mathbf{Q}$, indicated by the bold line in Fig. 5, determines the phase of the scattered wave. For plane wave scattering, the coordinates of atoms scattering with the same phase lie on 'Bragg planes', normal to $\mathbf{Q}$ and separated by a distance equal to $2\pi/Q$. Note that for atoms lying on any plane parallel to the Bragg planes, the in-plane coordinates do not alter the phase of the scattered amplitude.

Rotating the specimen, or the angle of incidence, over all orientations gives the isotropically averaged intensity, $I(Q)$. This is usually obtained much more conveniently through the Debye equation by assuming an isotropic distribution of atom density $\rho(r)$ at distance r from a chosen origin atom. Then, for a monatomic solid containing N atoms:

$$I(Q) = Nb^2\left[1 + 1/Q\int_0^\infty 4\pi r(\rho(r)-\rho_0)\sin(Qr)\,dr\right]. \tag{5}$$

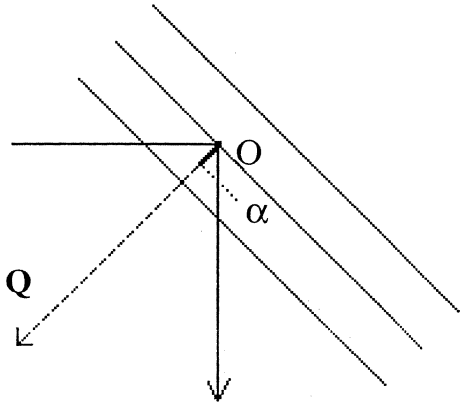

Fig. 5. Schematic representation of neutron scattering, for (vector) $\mathbf{Q}$, from atoms O and α. The waves scattered from O and α differ by a phase factor $\exp i(\mathbf{Q}\cdot\mathbf{r}_\alpha)$, where $\mathbf{r}_\alpha$ is the position vector of α with respect to O, and the magnitude of $\mathbf{Q}\cdot\mathbf{r}_\alpha$ is illustrated by the bold line.

Silicon crystallizes in the diamond cubic lattice with cell constant $a_0 = 0.5431$ nm. $S(Q_1)$ is indexed as a $\{1\,1\,1\}$ reflection with $d_{111} = (3)^{-1/2}a_0 = 0.314$ nm. $Q_1 = 2\pi/d_{111} = 20.04\ \text{nm}^{-1}$. Peaks at the d_{111} distance, and most multiples of d_{111} are absent in $G(r)$ – the exception being integer multiples of $3d_{111}$. The inter-planar d_{111} distance is specified by combinations of second-, third- and higher-neighbor distances involving atoms lying on $\{1\,1\,1\}$ planes. Taking d_{111} to be the apex – base distance of Si–Si_4 tetrahedra, the shortest distances in $G(r)$ which define the first plane are $(2)^{-1/2}\ a_0$ (=0.383 nm) and a_0 (=0.5431 nm). These are second and fourth neighbor distances. (The 0.383 nm distance is related to d_{111} through the angle between $\langle 1\,1\,1\rangle$ and the position vectors of atoms with fractional coordinates $(1/2, 1/2, 0), (1/2, 0, 1/2)\ldots$) Similarly, the second d_{111} plane (0.627 nm) is defined by fourth and higher neighbors, the shortest being $(3/2)^{-1/2}a_0$ (=0.665 nm) and $(2)^{-1/2}a_0$ (=0.768 nm). $S(Q_1)$ is thus defined by the conjunction of a series of features in $G(r)$, the position and intensity of which determine the Q value, height and width in Q-space. The pattern in $G(r)$ represented by these features becomes clear once the lattice planes have been correctly identified – but is not obviously determinable directly.

It is difficult to identify similar patterns in $G(r)$ for a-Si (or for a-SiO_2) since all the features beyond about 0.6 nm are diffuse. However, the pattern of features in $G(r)$ for a-Si is *not inconsistent* with that exhibited by the crystal. Differences in real space, $G(r)$, near 0.5 nm for instance, show that the structure of the crystal can be no more than a guide, however.

In framework structures like silica and many silicates, high contrast occurs when strongly scattering atoms lie on Bragg planes (with or without crystalline ordering). Voids and atoms that scatter neutrons with a phase shift of π (with or without crystalline ordering) between these planes would contribute to the scattered intensity. Such structures could result from a preferred distribution of large rings (with the same caveat). This demonstrates that the three models: voids, rings and quasi-lattice planes currently seen as competing explanations for low-Q structure, are in fact intimately related, and the alternative descriptions may be little more than a question of taste.

The key question that now arises is whether fluctuations in atomic density correspond to unconstrained randomness, or whether there are constraints implying order. If the latter; is the order basically crystallographic – possibly related to a corresponding crystalline phase? Or non-crystallographic relating to aperiodic structures based on pentagonal symmetry, for example?

4. LQS in unconstrained, random arrangements

Evidence relating to random medium-range structures, expressed in oxide glasses as random arrangements of local structural units, comes from the success or otherwise of continuous random network models. The well-known difficulties of providing reasonable fits to the low-Q structures in a-SiO_2 and a-GeO_2 and the relative paucity of models for other oxide glasses (apart from RMC simulations) suggests that unconstrained medium-range structures are likely to be unsuccessful. Models certainly do exist which provide good fits to experiment – such as those devised by Gladden [14]. But these contain constraints, on the ring size distribution for example.

Other evidence comes from recent work of Voloshin et al. [15]. They used a 27000 atom, dense random packed model with voids introduced by withdrawing atoms according to a pre-set pattern. A set of centers was chosen and atoms were withdrawn which lay within a sphere of radius δ. Several models were made with values of δ such that 15% of the atoms were removed in patterns ranging from crystal-like (face-centered cubic packing) to a completely random array. The former pattern of voids gave a pre-peak (and satellites) as expected, Fig. 6. The random pattern showed no pre-peak – merely a broad continuum of 'small angle scattering'.

A third pattern gave another interesting result. The pattern was based on a dense 'non-crystalline' packing of spheres interacting via a Lennard–Jones 6–12 potential. Voids arranged in this way produced a pre-peak in $S(Q)$, in almost the same position as that shown by the crystalline packing, although distinctly broader. Several

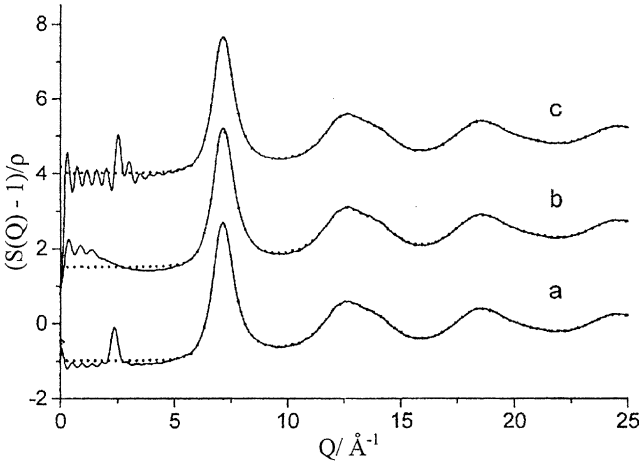

Fig. 6. Scattering from a model containing 27000 atoms dense randomly packed, but with 15% of the atoms removed to create voids according to a set pattern (Voloshin et al. [15]). In the upper diagram (c) a crystalline pattern was imposed whereas (b) was completely random. Note the presence of a pre-peak at about 2.5 Å^{-1} (25 nm^{-1}) in the model with a crystalline collection of voids, but only a broad continuum of 'small angle scattering' for the random arrangement. The lower diagram, (a) shows a pre-peak for a pattern of voids with similar characteristics to the atom positions in a dense random packed array. It is known that dense random packing involves considerable degree of constraint on interstice geometry and this seems to be sufficient to generate a pre-peak near 2.5 Å^{-1}. (1 Å ≡ 0.1 nm; 1 $\text{Å}^{-1} \equiv 10\ \text{nm}^{-1}$).

authors have pointed out that dense sphere packing with hard inter-atomic potentials introduces significant constraints. A high proportion of local arrangements are based on tetrahedral or octahedral packing. Secondly, a significant number of clusters are based on face-sharing tetrahedral packing with local pentagonal symmetry, which precludes periodic Euclidean space-filling. This is perhaps the only clue I can offer in favor of the view that a more extensive non-crystallographic medium-range structure may satisfactorily explain low-Q structure.

Summarizing the position thus far. Completely random models for the medium-range structure seem unlikely candidates for an adequate representation of LQS in simple oxide glasses. The possibility that non-crystallographic ordering may be implicated requires further examination. I now consider the case for models based on equivalent crystalline structures.

5. LQS in models with medium-range ordering based on crystal models

In complete contrast to the paucity of evidence for non-crystallographic ordering, there is no shortage of evidence for, and against, the proposition that medium-range ordering in amorphous solids is based on similar principles to those exhibited by corresponding crystals.

Gaskell and Wallis [13] calculated the *anisotropic* scattering, $S(\mathbf{Q})$ for $|\mathbf{Q}| = Q_1$, from models for a-SiO_2 using the method described by Alben et al. [16]. They concluded that the *highest values* of the anisotropic intensity, in those models that were most successful in describing the FSDP in silica, were associated with planar fluctuations in atomic density. These showed similarity with {1 1 1} planes in cubic cristobalite, and were termed 'quasi-lattice planes'. It was emphasized that these should *not* be considered as (two-dimensional) 'layers', and that a microcrystallite model is *not* implied. (These warnings have subsequently been ignored by others who have looked for and found neither 'layers' nor crystallites.)

Quasi-lattice planes in silica are similar, but less prominent than those described by Alben et al. who demonstrated planar ordered regions in DRHPS models. More recently, Mountjoy [17] examined spherical regions containing about 500 atoms in large (~14 000 atoms) models for amorphous tetrahedral carbon (derived from large models for a-Si). Significantly ordered crystal-like regions were found, (Fig. 7), with high values of $I(\mathbf{Q})$ well beyond those predicted for 'random' isotropic scattering.

If the peak intensity values of the anisotropic scattered intensity can be ascribed to *recognizable* medium-range features ({1 1 1} planes in the case of silica) then it is reasonable to test the hypothesis that similar,

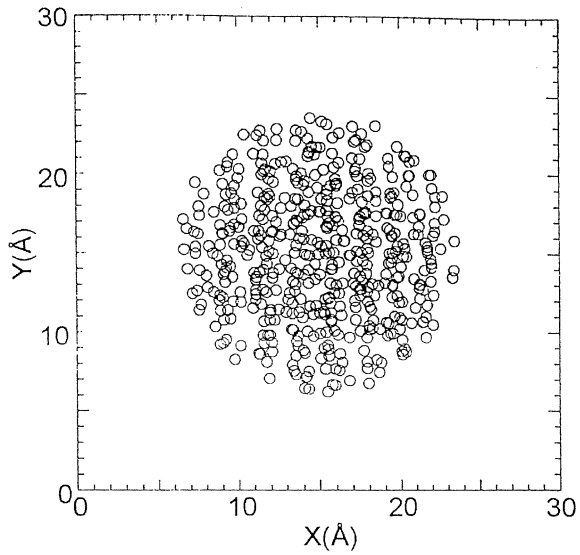

Fig. 7. Planar atomic density fluctuations parallel to Y observed by Mountjoy [17] at maximal values of the anisotropic scattering intensity, $I(\mathbf{Q})$ from 500-atom spherical regions of a 14 000 atom model for amorphous tetrahedral carbon re-scaled from a model constructed for a-Si.

but much less obvious, *crystal-like* medium range structural features may be responsible for the less intense contributions of $S(\mathbf{Q}_1)$ to the average, $S(Q_1)$. Through the negative exponential statistics associated with $I(\mathbf{Q})$, the lower values of $I(\mathbf{Q})$ sum to give the *largest* contributions to the averaged FDSP, $S(Q_1)$. The hypothesis then is: that medium-range structure associated with a significant volume of a macroscopic specimen has the *essential medium-range character* of the crystal. And that the LQS data for the glass and the equivalent crystal, are similar and arise for the same reasons. This assertion clearly demands proof. It would be equally (or more) plausible to present the counter argument. Namely, that the ease of formation by quenching from the melt, and the relative stability to crystallization, implies that amorphous solids have structures that are *essentially different* from those of the corresponding crystals.

The close similarity between the values of Q_1 for the glassy, crystalline and (sometimes) liquid forms of a material has been noted by several authors. What is perhaps more surprising is that in those cases where there are several components of the LQS, some of the details mirror the LQS of a corresponding crystal. Moreover, interpretation is relatively obvious and the method easy to perform.[1] Here I give one set of examples: LQS in alkali disilicate glasses, $M_2 \cdot (Si_2O_5)$.

[1] Using Cerius software (Accelerys, 334 Science Park, Cambridge, UK).

5.1. LQS in alkali disilicate glasses

Specifying what is meant by 'essential medium-range character' needs care. One description is in terms of 'structure-forming operations' (SFOs) – that is the set of operations that produce the medium-range structure of the crystal and, hypothetically, that of the glass (see Gaskell 1995) [18]. Briefly, SFOs for disilicate glasses involve corrugated, two-dimensional sheets of six-membered rings of $Si_2O_5^{2-}$ units parallel to {0 1 0} with alkali ions, M^+, occupying the inter-planar spaces. The degree of corrugation of the disilicate sheets depends on the size of the alkali cation and its coordination number.

Low-Q structures in neutron scattering data from several disilicate glasses, with M = ^{nat}Li [19,20], K/^{nat}Li [21] and Na [22] are shown in Fig. 8. On the same diagram, simulated neutron scattering data are given for the corresponding crystals [23]. Crystallites, 2 nm in size were chosen to give a crude estimate of the effects of disorder; without implying a microcrystallite model, of course. The strong feature around 17–18 nm^{-1} seen in all materials, glassy or crystalline, is indexed as a {1 1 1} crystal reflection. Fig. 9 shows that in c-$Li_2Si_2O_5$,

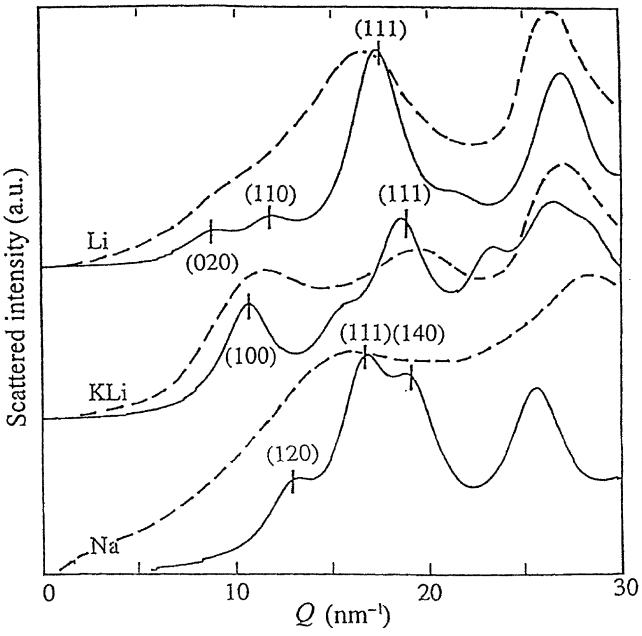

Fig. 8. Experimental LQS neutron scattering data for disilicate glasses containing Li, K/Li and Na [19–22] (dashed lines). Simulated neutron scattering data [23] are also shown (full line). Absolute intensities are arbitrary but comparable. In the sequence Li, K/Li, Na, ratios are: 1.0:0.72:0.82. Experimental scattering intensities are also arbitrary. Recent measurements [25] of neutron scattering from a-$Na_2Si_2O_5$ at 400 K have shown a very weak shoulder at about 10–12 nm^{-1} at 400 K, which becomes more prominent in the melt at 1600 K. Horbach et al. [26] associate this with peaks in the Na-centered partial structure factors calculated for a molecular dynamics simulation of the melt. I am grateful to Jürgen Horbach for pointing this out.

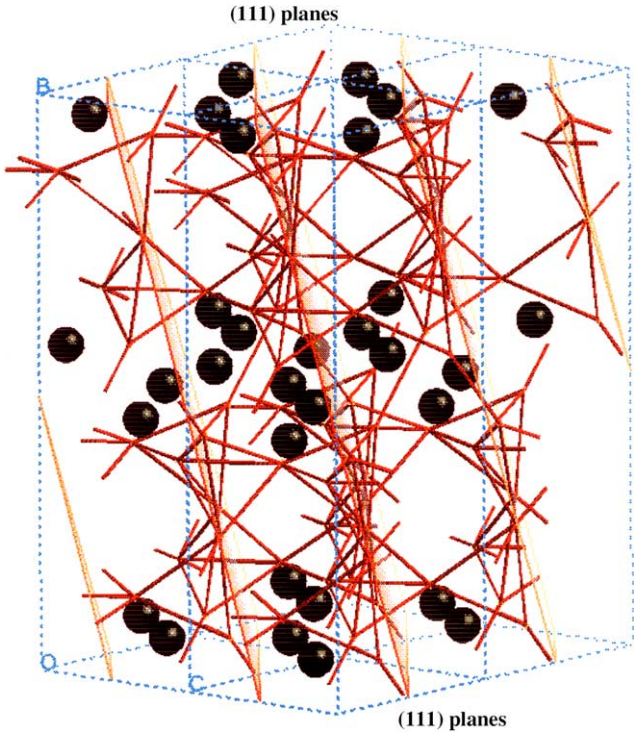

Fig. 9. The crystal structure of $Li_2Si_2O_5$ [24] showing planes parallel to (1 1 1) which are associated with the strong peak near 18 nm^{-1} in Fig. 8. Note that these planes link SiO_4 tetrahedra that form the corrugated layers, separated by planes rich in Li^+ ions (spheres). Note also that the latter are fairly evenly scattered in directions normal to the (1 1 1) planes.

[24] planes parallel to (1 1 1) pass through regions of high Si and O atom density and follow the edges of the interconnected rings of tetrahedra that make up the disilicate sheets. From another view, these planes connect the corrugated layers. The planes in the crystal are thus defined by the geometry of the six-membered rings, the extent of puckering of the sheets and by the relative disposition of neighboring layers.

In the glass, disorder will modify the medium-range structure and therefore affects the LQS. A reasonable assumption would be that the amount of distortion reflects the relative strengths of the relevant chemical bonds. Intra-planar distortions would therefore be expected to be much smaller than inter-planar distortions. The former are controlled by strong, directional Si–O bonds and the latter by weak, central, M^+–O^- interactions. Thus the effects of disorder on the (1 1 1) peak in translating from the crystal to the glass are likely to be relatively minor. However, features at lower values of Q are associated with inter-planar distances, such as (0 2 0) in $Li_2Si_2O_5$ and (1 0 0) planes in $LiKiSi_2O_5$, Fig. 10. Variations in inter-planar spacings and the registry between neighboring planes would be expected to lead to broad diffuse peaks in the LQS and this is seen in the experimental data. Overall, the agreement with the details of the low-Q structure is good for the positions

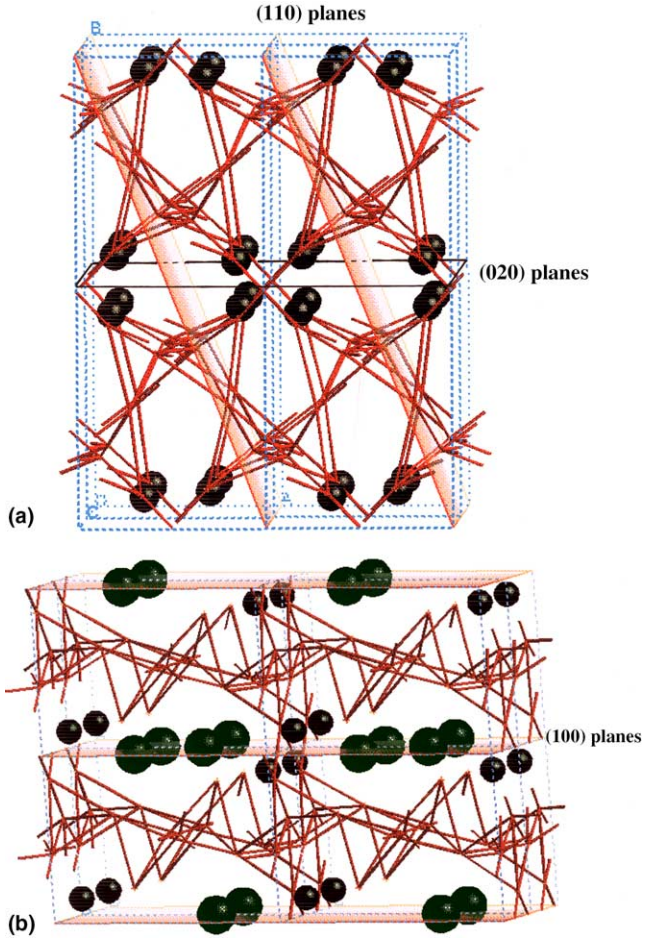

Fig. 10. (a) Crystal structure of: $Li_2Si_2O_5$ projected along [100] showing corrugated layers of Si_2O_5 units, separated by (020) planes rich in Li^+ ions (black spheres). (020) planes (horizontal) and (110) (inclined) are associated with weak features in LQS data near 10 nm^{-1} in Fig. 8. (b) Structure of c-$KLiSi_2O_5$ [21] showing that large K^+ ions cause the $Si_2O_5^{2-}$ layers to become flatter. Horizontal (100) planes are shown, associated with the peak near 11 nm^{-1} in Fig. 8.

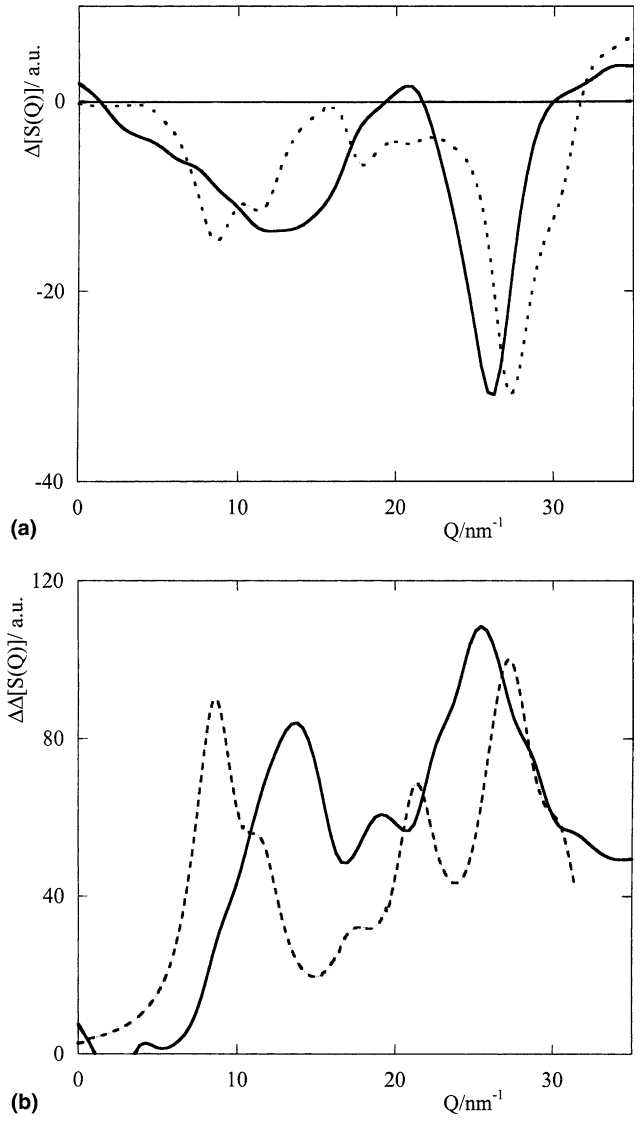

Fig. 11. (a) Experimental 'first difference' data obtained by Zhao et al. [19] by subtracting $S(Q)$ data for two disilicate glasses containing ^7Li and ^6Li. The difference, $\Delta[S(Q)]$, (^6Li–^7Li) gives a weighted sum of the Li-centered partial structure factors only. Simulated data are also shown (dashed line). (b) Experimental 'double difference' data, $\Delta\Delta[S(Q)]$, obtained by Zhao et al. [19] from neutron scattering data from specimens of lithium disilicate glasses with three concentrations of ^6Li and ^7Li. The resultant is proportional to the Li–Li partial structure factor. Simulated data are also shown (dashed line). (Simulated Na–Na correlations in a-$Na_2Si_2O_5$ are very similar.) Note the reasonable representation of experimental data in both (a) and (b) above about 15 nm^{-1}. However, agreement at lower values of Q is poor.

of the major features with the intensities, not surprisingly, much less reliable.

Zhao et al. [19] have also obtained data for the contribution of Li-centered partials to the structure factor in a-$Li_2Si_2O_5$ from neutron scattering data with isotopic substitution of Li. 'First difference' data give a weighted sum of Li–O, Li–Si and Li–Li partials. These data are compared with simulations based on c-$Li_2Si_2O_5$ in Fig. 11(a). The single difference experimental data, $\Delta S(Q)$, is obtained as the difference between scattering data for glasses containing ^6Li, which has a normal positive scattering length; and ^7Li, which has a negative scattering length. Negative values of $\Delta S(Q)$ reflect lower scattering intensities from the ^6Li-containing glass. Such negative values are the result of Li atoms sited between the regions with high atomic densities of Si and O, which make the major contribution to the (total) scattered intensity. In the crystal models, ^6Li atoms (which scatter normally) lying between Bragg planes that are highly populated by Si and O (the (002) plane, for example, Fig. 10) reduce the (total) scattered wave amplitude. In this case, the contribution from ^6Li to the scattering is out of phase with that of the contributions from Si and O. The ^7Li isotope, however, scatters in antiphase compared with the other atoms, so that for the same **Q** vector, the total scattering amplitude is *increased*.

The simulation correctly reproduces the experimental difference data in the region of the strongest low-Q peak at about 17 nm^{-1} where differences between the intensities scattered by the ^{6}Li- and ^{7}Li-containing glasses are small. In the simulation the intensity corresponds to (1 1 1) and (1 4 0) scattering and in both cases Li atoms are fairly evenly distributed along and between the planes (see Fig. 9).

The first component of the experimental LQS difference data is poorly reproduced by the crystal model. The simulation suggests two peaks corresponding to the (0 2 0) reflection at about 9 nm^{-1} and (1 1 0) scattering at about 11 nm^{-1}. The experimental $\Delta S(Q)$ data shows a negative-going maximum at about 13 nm^{-1}. It is possible to appeal to the effect of disorder which will reduce inter-planar (0 2 0) scattering but, even so, the fit would not be impressive.

Fig. 11(b) displays experimental 'second difference' data, $\Delta\Delta S(Q)$, giving a representation of the Li–Li partial structure factor. The latter is obtained from very small intensity differences between the much larger intensities corresponding to the total scattering from each of three glasses. The data are therefore subject to a high level of random noise and to potentially large systematic uncertainties. This simulation is most accurate in the region near 19 nm^{-1}, where the absence of Li–Li contributions to the scattered intensity is shown both in experimental and simulated data. The model fails again, this time more seriously, to reproduce the lowest Q peak at about 14 nm^{-1} in the experimental $\Delta\Delta S(Q)$ data. Appeal to disorder-induced broadening of the (0 2 0) peak would help, but simulation using the crystalline model fails to predict the inter-planar Li–Li distances, which appear to be shorter in the glass, even though transformation [19] of the $\Delta\Delta S(Q)$ double difference data shows that the nearest-neighbor Li–Li distances are similar in glass and crystal [24].

The conclusion must be, however, that while the crystal model adequately predicts the scattering from Si and O atoms making up the corrugated layers, it fails to give a realistic guide to the positions of the weakly-bonded Li^+ ions.

6. Conclusions

This paper has attempted to show that the precise language used to describe the structural origins of low-Q structure in glasses is less important than the fact that atomic density fluctuations are spatially correlated. Voids, rings quasi-lattice planes are all useful descriptors of medium-range structure and associated density fluctuations. The principal issue with LQS remains the fact that some form of non-random correlation in atomic density extends to distances of the order 1.5 nm. It is not yet clear what the origin of this non-random correlation might be.

One possibility is that viable potential energy functions may require a long-range energy term, which predisposes the relative positions of atoms separated from each other by distances of the order 10 times the nearest-neighbor separation. Coulombic terms may be a possibility for ionic solids, but this cannot answer problems raised by LQS in amorphous elemental materials like a-Si and a-Ge. Given such long-range terms, the preferred solution then emerges through energy minimization, in the same way that the crystal structure is defined by (presumably similar) energy terms. Relations between medium-range structure of glasses and equivalent crystals then become more obvious.

A second possibility is that the structure of amorphous materials is primarily determined by topological constraints. The requirement for energy minimization – even if the potential energy contains only local terms – restricts the number of unsatisfied bonds, so that network continuity becomes a paramount factor. In DRHPS structures, the requirement to pack atoms efficiently introduces extensive restrictions in interstice geometry. Similar constraints must operate in network glasses – especially if the mean atomic density, ρ_0, is specified as a constraint. This type of explanation has considerable force and is supported by the observation of 'extended-range ordering' by Uhlherr and Elliott [3], mentioned earlier in connection with models for a-Si. Such oscillations in $\rho(r)$ are extremely weak and appear to be too small to provide a complete answer. However, topological ordering, in ostensibly random models, seems likely to contribute to a solution of the mystery.

In the meantime, crystal models for the medium-range structure provide perhaps the most useful (but not infallible) guide. Again, it should be stressed that the degree of 'crystal-like' ordering is only marginal. The normalized variance of the anisotropic scattering is only fractionally greater than the statistics of random models predict. There is no suggestion that quasi-lattice planes must be observable at every atom site. Merely that there is a predisposition towards a medium-range structure that is recognizable through the structure of equivalent crystals.

Perhaps the most useful final comment might be that experimental techniques such as high resolution transmission electron microscopy or scanning transmission electron microscopy which probe the variability, or granularity, of the structure on a microscopic scale, will acquire much greater importance in future work. This may entail some demotion of techniques like neutron and X-ray scattering which deal with orientationally-averaged properties and emphasize isotropy at all levels beyond the local structure. But, after all, these techniques have already provided most of our knowledge of the detailed structure of glasses and other amorphous solids.

Acknowledgments

I am indebted to Jianguo Zhao, David Wallis and Gavin Mountjoy for contributions to the work mentioned here and for useful discussion. Also to Adrian Wright and Sjoerd Roorda for experimental neutron and X-ray scattering data for a-SiO_2 and a-Si and to Alistair Cormack for several fruitful discussion.

References

[1] G. Etherington, A.C. Wright, J.T. Wenzel, J.C. Dore, J.H. Clarke, R.N. Sinclair, J. Non-Cryst. Solids 48 (1982) 265.
[2] K. Laaziri, S. Kycia, S. Roorda, M. Chicoine, J.L. Robertson, J. Wang, S.C. Moss, Phys. Rev. 60 (1999) 13520.
[3] A. Uhlherr, S.R. Elliott, J. Phys.: Condens. Matter 6 (1994) L99; Philos. Mag. 71 (1995) 611.
[4] J.M. Holender, G.J. Morgan, J. Phys.: Condens. Matter 3 (1991) 1947; 7241.
[5] A.H. Narten, C.G. Venkatesh, S.A. Rice, J. Chem. Phys. 64 (1976) 1106.
[6] S.R. Elliott, J. Chem. Phys. 103 (1995) 2758.
[7] D.R. Barker, M. Wilson, P.A. Madden, N.N. Medvedev, A. Geiger, Phys. Rev. E 62 (2001) 1427.
[8] For a recent review see: X. Yuan, A.N. Cormack, J. Non-Cryst. Solids 319 (2003) 31.
[9] A.C. Wright, R.N. Sinclair, J. Non-Cryst. Solids 76 (1985) 351.
[10] S. Wefing, J. Non-Cryst. Solids 244 (1999) 89; 113.
[11] J.A.E. Desa, A.C. Wright, R.N. Sinclair, J. Non-Cryst. Solids 99 (1988) 276.
[12] J.A.E. Desa, A.C. Wright, J. Wong, R.N. Sinclair, J. Non-Cryst. Solids 51 (1982) 57.
[13] P.H. Gaskell, D.J. Wallis, Phys. Rev. Lett. 76 (1996) 66.
[14] L.F. Gladden, J. Non-Cryst. Solids 119 (1990) 318.
[15] V.P. Voloshin, S. Beaufils, N.N. Medvedev, J. Mol. Liq. 97 (7) (2002) 101.
[16] R. Alben, G.S. Cargill III, J. Wenzel, Phys. Rev. B 13 (1976) 835.
[17] G. Mountjoy, J. Non-Cryst. Solids 293–295 (2001) 458.
[18] P.H. Gaskell, J. Non-Cryst. Solids 192 & 193 (1995) 9.
[19] J. Zhao, P.H. Gaskell, M.M. Cluckie, A.K. Soper, J. Non-Cryst. Solids 234 (1998) 721.
[20] H. Uhlrig, M.J. Hoffmann, H.-P. Lamparter, F. Aldinger, R. Bellissent, S. Steeb, J. Amer. Cer. Soc. 79 (1992) 2833; A.C. Hannon, B. Vessal, J.M. Parker, J. Non-Cryst. Solids 150 (1992) 97.
[21] B.H.W.S. de Jong, H.T. Supℵr, Acta Crystallogr. B 52 (1996) 770.
[22] M. Misawa, D. Price, K. Suzuki, J. Non-Cryst. Solids 37 (1980) 85.
[23] P.H. Gaskell, Mineral. Mag. 64 (2000) 425.
[24] F. Liebau, Acta Crystallogr. B 24 (1968) 13.
[25] A. Meyer, H. Schober, D.B. Dingwell, Europhys. Lett. 59 (2002) 708.
[26] J. Horbach, W. Kob, K. Binder, J. Phys.: Condens. Matter 15 (2003) S903.